Chemical Engineering Journal 145 (2008) 69–77

Contents lists available at ScienceDirect

Chemical Engineering Journal

journal homepage: www.elsevier.com/locate/cej

Hydrodynamic modeling of a novel multi-stage gas–liquid external loop airlift reactor

S. Sarkar[a], Kaustubha Mohanty[b], B.C. Meikap[a,*]

[a] Department of Chemical Engineering, Indian Institute of Technology, Kharagpur 721302, India
[b] Department of Chemical Engineering, Indian Institute of Technology Guwahati, Guwahati 781039, India

ARTICLE INFO

Article history:
Received 29 October 2007
Accepted 12 March 2008

Keywords:
Multi-stage external loop airlift reactor
Hydrodynamic model
Gas holdup
Gas–liquid contactor
Liquid circulation velocity

ABSTRACT

A mathematical model for predicting the hydrodynamic behavior of a multi-stage external loop airlift reactor operating in three stages has been developed. The present model is based on macroscopic balances of the gas–liquid separator, external downcomer and spatially averaged, 1D mass and momentum balances in the riser. Using only the physical properties of the gas and liquid phases, the reactor dimensions and the superficial gas velocity, the model predicts gas holdup profiles, gas and liquid velocity profiles, and pressure profiles in the riser for a two-phase bubbly flow. It has been observed that the values of gas holdup obtained are in the range of 44–52%. Empirical correlations are used to represent frictional and drag effects, but there are no adjustable parameters in the model. Results indicate that a pressure of 9.3×10^{-4} N/m^2 were achieved at a dimensionless riser position of 1.0. The results predicted by the model are in excellent agreement with the experimental data reported in literature for a multi-stage external loop airlift reactor.

1. Introduction

Airlift reactors have been used in many process industries where compressed air is used to simultaneously aerate and agitate the liquid with controlled recirculation. Because of their simple construction and operation and their defined mixing and intensive dispersing effects with relatively low power requirements, airlift reactors are frequently used in chemical and biochemical industries. They are particularly well-suited for processes with demands for rapid and uniform distribution of the reaction components, e.g. neutralization of wastewater, and for multiphase systems for which high mass and heat transfer are necessary, e.g. fermentation processes [1–5].

Different designs of airlift reactors have been studied earlier by many investigators, but most of them operate in a single stage. Some of the reactors, in which different internals like baffles, plates and screens were used to increase the efficiency, resulted in high energy dissipation and complex mechanical construction leading to difficulty in construction and operation. To achieve higher efficiency, the airlift reactors must be operated in multi-stage. Mohanty et al. [5] has designed a novel multi-stage external loop airlift reactor by exploiting the hydrodynamics of a buoyancy-induced two-phase flow. The staging effect was achieved through hydro-dynamically induced continuous bubble generation, break up and regeneration, so that in each stage completely de-aerated liquid could be brought in contact with freshly generated bubbles. The details of the design and characterization of this reactor is reported elsewhere [5].

Several models describing satisfactorily the hydrodynamics of two-phase airlift reactors have been developed [6–9]. Some of the models are based on drift–flux theory [10] and macroscopic energy balances [11,12]. Other models are based on mechanical energy balances and empirical correlations for the parameters that represent viscous dissipation effects [6,13]. Recent models have used the momentum equations to describe spatial variations of the hydrodynamic variables. Some of these models consider two-dimensional representations of velocity and gas holdup profiles [14], whereas others consider only axial variations of these parameters [15–17].

Another approach for investigating airlift fluid mechanics has been the application of an energy balance to the expanding, isothermal sparging gas. The total expansion work done by the gas is equated to the sum of various sources of energy dissipation [6].

Models derived from this type of analysis have been successful in predicting the liquid-phase velocity, provided the gas volume fraction is known.

Most models of airlift hydrodynamics have assumed the flow to be homogenous, i.e., without variation between phases or spatial position. However, it is apparent that the two-phase flow characteristics of airlift reactors are not homogenous always. Significant differences in phase velocities are the norm, and distinct variations

* Corresponding author. Tel.: +91 3222 283958; fax: +91 3222 282250.
E-mail addresses: kmohanty@iitg.ernet.in (K. Mohanty), bcmeikap@che.iitkgp.ernet.in (B.C. Meikap).

1385-8947/$ – see front matter © 2008 Elsevier B.V. All rights reserved.
doi:10.1016/j.cej.2008.03.007

Nomenclature

A	cross-sectional area of flow channel (m^2)
A_g	cross-sectional area of riser occupied by gas phase (m^2)
C_D	bubble drag coefficient
C_0	drift–flux theory distribution parameter
D	diameter (m)
f	friction factors
F_b	drag force per unit gas/liquid interfacial area
F_D	drag force per bubble
g	gravitational acceleration (m/s^2)
G	gas mass flux (kg/m^2 s)
ht	depth of liquid in the separation tank (m)
I	liquid turbulence intensity
j	superficial mixture velocity (m/s)
j_g	superficial gas velocity (m/s)
k	excess pressure drop due to developing flow effects (N/m^2)
L	axial distance from sparger to riser (m)
$\dot{L}$	liquid mass flux (kg/m^2 s)
m, n	exponents
M	molecular weight of gas (amu)
n	unit normal vector
P	pressure (N/m^2)
Q	volumetric flow rate (m^3/s)
r	radial coordinates, radius
R	outer tube radius (m)
Re	Reynolds number
T	temperature (°C)
U	uniform velocity profile at flow channel entrance (m/s)
U_g	gas superficial velocity, based on riser cross-section and atmospheric pressure (m/s)
v	fluid velocity (m/s)
z	axial component
$\langle\ \rangle$	volume average

Greek letters

α	weighting factor
$\bar{\alpha}$	time average of the quantity α
α'	deviation from time average
ε	phase volume fraction
ε_g	void or gas fraction
ξ	axial length of flow development zone
θ	azimuthal component
μ	viscosity
ρ	liquid density
σ	gas/liquid interfacial tension
τ	viscous stress tensor
$\widehat{\psi}$	area average of ψ
$\breve{\psi}$	deviation from area average
$\tilde{\psi}$	deviation from volume average

Subscripts

atm	atmospheric
b	bubble
c	center of tube
dc	downcomer
g	gas
gl	gas/liquid interface
l	liquid
r	riser
s	sparger
t	separation tank
w	wall
z	axial coordinate

Superscripts

t	turbulent
T	transpose
(T)	total

in void fraction and phase velocity occur with changes in radial position. Additionally, for large-scale applications, changes in fluid velocities and gas fractions with axial position are expected to be substantial. In this study, a model was developed for a two-phase flow, which takes into account the changes occurring between phases and axial positions. The hydrodynamic parameters predicted by this model were matched with the experimental data reported in literature for a multi-stage external loop airlift reactor [5].

2. Development of the model

In the present investigation the hydrodynamic model is developed from fundamental continuity, momentum and energy balance equations in the riser, downcomer and separator. In the process, the two-phase frictional effects like riser wall friction, gas–liquid drag force and downcomer wall friction factor has been considered. The effect of buoyant forces in the gas and liquid momentum balances has also been taken into consideration.

2.1. Assumptions

In this model, starting from the time-averaged point equation of continuity for each phase, an averaging process over a representative volume of gas–liquid suspension is carried out. The volume-averaged equations are then averaged over the cross-section of the riser. The following assumptions were made for simplification of the complex system:

- Steady state operation.
- Chemical reactions are absent.
- Gas is ideal.
- Uniform liquid density, i.e., incompressible flow.
- Negligible gas–liquid mass transfer.
- Flow is under isothermal conditions.
- Bubbly flow in the riser, i.e., the superficial gas velocity in the riser section is low enough. Gas bubbles move uniformly upward, and there is negligible bubble dispersion with limited coalescence and breakup.

2.2. Riser

The schematic diagram of the multi-stage external loop airlift reactor is shown in Fig. 1. The details of the experimental methods of measurement of gas holdup, liquid circulation velocity is reported elsewhere [5].

2.2.1. Continuity equation

The time-averaged, steady-state continuity equation has the form: $\nabla \cdot \rho v = 0$.

Employing the definition of the volume average for any variable ψ over some arbitrary averaging volume V_a,

$$\langle\psi\rangle_a \equiv \frac{1}{V_a}\int_{V_a} \psi \, dV. \quad (1)$$

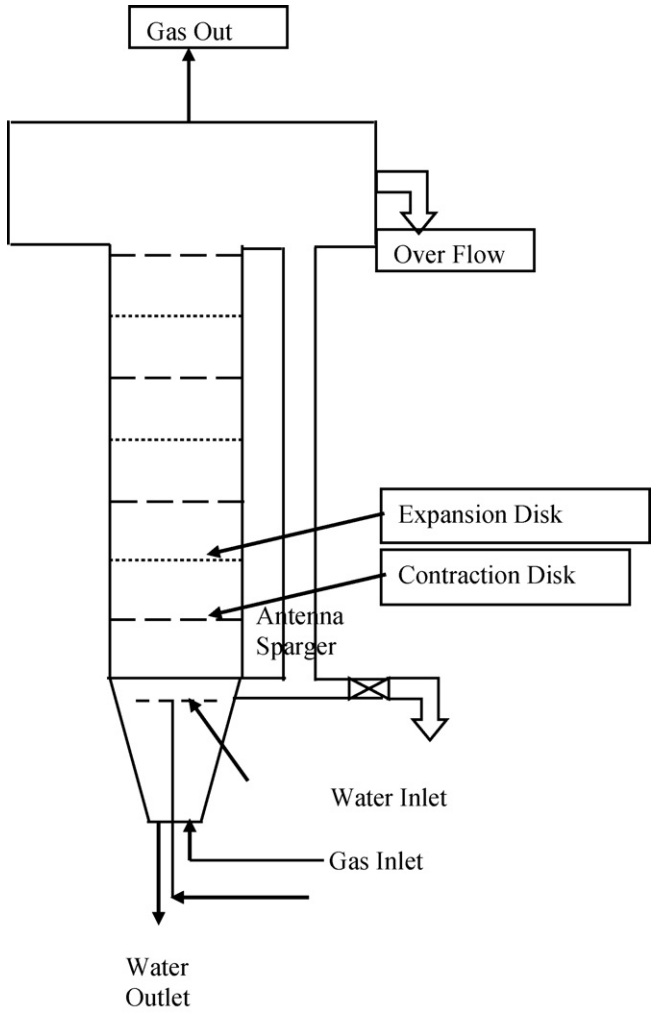

Fig. 1. Schematic diagram of the multi-stage external loop airlift reactor experimental set-up.

The volume-averaged continuity equation becomes:

$$\frac{1}{V_a}\int_{V_a}[\nabla\cdot(\rho v)]\,dV = 0. \tag{2}$$

The averaging volume includes both gas and liquid. Since the liquid-phase equation is being considered, the limits of integration may be rewritten in terms of the liquid volume V_l, rather than the total volume,

$$\frac{1}{V_a}\int_{V_l}[\nabla\cdot(\rho v)]\,dV = 0. \tag{3}$$

The spatial-averaging theorem for some liquid vector property a,

$$\int_{V_l}\nabla\cdot a\,dV = \nabla\cdot\int_{V_l} a\,dV + \int_{A_{gl}} a\cdot n\,dA \tag{4}$$

may be applied, where A_{gl} represents the gas–liquid interfacial area. The resulting form of the volume-averaged continuity equation is,

$$\nabla\cdot\langle\rho v\rangle + \frac{1}{V}\int_{A_{gl}}(\rho v)\cdot n\,dA = 0. \tag{5}$$

The second term on the left-hand side represents the mass flux between gas and liquid. Assuming mass transfer to be negligible, the continuity equation can be written as,

$$\nabla\cdot\langle\rho v\rangle_a = 0. \tag{6}$$

The average based on the averaging volume is related to the interstitial (i.e., physical) averaging in the following manner:

$$\langle\rho\rangle_a = (1-\varepsilon)\langle\rho\rangle. \tag{7}$$

Substitution into the continuity equation gives,

$$\nabla\cdot(1-\varepsilon)\langle\rho v\rangle = 0. \tag{8}$$

To rewrite the average of the product of density and velocity, the quantities of interest may be expressed as the sum of the mean value and a deviation (denoted by the tilde),

$$\rho = \langle\rho\rangle + \tilde{\rho} \quad \text{and} \quad v = \langle v\rangle + \tilde{v}. \tag{9}$$

By taking the product of these expressions and averaging the results over the liquid phase, it can be shown that,

$$\langle pv\rangle = \langle\rho\rangle\langle v\rangle + \langle\tilde{\rho}\tilde{v}\rangle. \tag{10}$$

It can be noted that this simplification is due to the fact that, the definition of the average of the deviations is zero. By assuming that average values are much greater in magnitude than deviations, the product of deviations becomes negligibly small compared to the product of averages. Hence, the volume-averaged liquid continuity equation may be written as,

$$\frac{d}{dz}[(1-\varepsilon)\langle\rho\rangle\langle v\rangle_z] + \left(\frac{1}{r}\right)\frac{d}{dr}[r(1-\varepsilon)\langle\rho\rangle\langle v\rangle_r] = 0. \tag{11}$$

The area average of some fluid property ψ is defined as,

$$\bar{\psi} \equiv \frac{1}{A}\int_A \psi\,dA, \tag{12}$$

where A is the cross-sectional area of the flow channel. By applying the averaging formula to the continuity equation and observing that $\langle v\rangle_r = 0$ at the wall, the radial derivative term equals zero. The density is independent of radial position. The order of differentiation and integration may be reversed and the density may be removed from the area integral. The volume fraction and velocity may be written as the sum of the area average (denoted by the hat symbol) and deviation (denoted by the breve symbol):

$$1-\varepsilon = 1-\hat{\varepsilon}-\breve{\varepsilon}. \tag{13}$$

Substitution into the continuity equation and simplification yield,

$$\frac{d}{dz}\left[\langle\rho\rangle(1-\hat{\varepsilon})\langle\hat{v}\rangle_z\right] = 0. \tag{14}$$

This assumption introduces some error into the model in return for computational simplicity. However, the errors will not be large.

A parallel development for the gas phase produces a directly analogous result of the form:

$$\frac{d}{dz}\left[1-\langle\rho\rangle\hat{\varepsilon}\langle\hat{v}_g\rangle_z\right] = 0. \tag{15}$$

2.2.2. Momentum equations

The time-averaged point equations of motion for incompressible flow have the form,

$$\rho\left(\frac{\partial v}{\partial t} + v\cdot\nabla v\right) = -\nabla P + \rho g + \nabla\cdot\tau^{(T)}, \tag{16}$$

where $\tau^{(T)}$ is the sum of the viscous and turbulent stress tensors. Neglecting the convective acceleration and assuming steady-state operation, the volume-averaged momentum equation becomes,

$$\frac{1}{V_a}\int_{V_a}\{-\nabla P+\rho g+\nabla\cdot\tau^{(T)}\}\,dV=0. \tag{17}$$

Applying the spatial-averaging theorem to the pressure and stress tensor terms and writing the momentum equation for the liquid phase in terms of intrinsic phase average yields,

$$-\nabla(1-\varepsilon)\langle P\rangle+\frac{1}{V_a}\int_{A_{gl}}(-PI+\tau^T)\cdot n\,dA+(1-\varepsilon)\langle\rho\rangle g +\nabla\cdot(1-\varepsilon)\langle\tau\rangle^T=0, \tag{18}$$

where n is a unit vector normal at any given point on the surface of the gas–liquid interface. Expanding the volume-averaged stress tensor term results in the form,

$$\nabla\cdot(1-\varepsilon)\langle\tau\rangle^T=\nabla\cdot(1-\varepsilon)\langle\tau\rangle+\nabla\cdot(1-\varepsilon)\langle\tau^t\rangle, \tag{19}$$

where τ is the liquid viscous stress tensor $=\mu(\nabla v+\nabla v^T)$, $\langle\tau^t\rangle$ is the liquid turbulent stress tensor $=-\langle\overline{\rho v'v'}\rangle$, and ∇v^T is the transpose of the dyad ∇v.

The overbar on $-\langle\overline{\rho v'v'}\rangle$ indicates that the time average was done over the entire product. Volume averaging and applying the spatial-averaging theorem to τ yields,

$$\langle\tau\rangle=\mu\left[\nabla\langle v\rangle+\nabla\langle v\rangle^T\right]+\mu\left[\frac{1}{V_a}\int_{A_{gl}}nv\,dA+\frac{1}{V_a}\int_{A_{gl}}vn\,dA\right]. \tag{20}$$

Since the liquid velocity v is nearly uniform with respect to the position on the bubble interface and the unit normal vector integrates to zero over the surface, the area integrals are zero and

$$\langle\tau\rangle=\mu[\nabla\langle v\rangle+\nabla\langle v\rangle^T]. \tag{21}$$

Writing the volume average of the turbulent stress tensor as $\langle\tau^t\rangle=-\langle\overline{\rho v'v'}\rangle$, the equations of motion become,

$$-\nabla(1-\varepsilon)\langle P\rangle+\frac{1}{V_a}\int_{A_{gl}}(-PI+\tau^T)\cdot n\,dA+(1-\varepsilon)\langle\rho\rangle g +\nabla\cdot(1-\varepsilon)\mu[\nabla\langle v\rangle+\nabla\langle v\rangle^T]-\nabla\cdot(1-\varepsilon)\langle\overline{\rho v'v'}\rangle=0. \tag{22}$$

The remaining area integral term represents the total force exerted at the gas–liquid interface, i.e., the drag force between gas and liquid phases per unit volume plus the buoyancy forces. The term can be expressed as proportional to the total interfacial force acting on the liquid per unit gas–liquid interfacial area F_t,

$$a_{lg}F_t=\frac{1}{V}\int_{A_{gl}}(-P_lI+\tau_l^{(T)}\cdot n\,dA), \tag{23}$$

where A_{gl} is the gas–liquid interfacial area per unit volume of gas–liquid suspension.

To develop the one-dimensional model, the axial component of the momentum equation is taken. Expanding the viscous term gives,

$$\nabla\cdot(1-\varepsilon)\mu\left[\nabla\langle v\rangle+\nabla\langle v\rangle^T\right]=(1-\varepsilon)\mu\left[\nabla^{2\langle v\rangle}+\nabla(\nabla\cdot\langle v\rangle)\right] +\mu\left[\nabla\langle v\rangle+\nabla\langle v\rangle^T\right]\cdot\nabla(1-\varepsilon). \tag{24}$$

Noting that divergence of the velocity vector is zero and assuming that $\langle v\rangle_z=\langle v\rangle_z(r,z$ only), the axial component of the first term on the right-hand side becomes,

$$e_z\cdot(1-\varepsilon)\mu[\nabla^2\langle v\rangle]=(1-\varepsilon)\mu\left[\frac{1}{r}\frac{\partial}{\partial r}\left(r\frac{\partial\langle v\rangle_z}{\partial r}\right)+\frac{\partial^2\langle v\rangle_z}{\partial z^2}\right], \tag{25}$$

where e_z is the unit vector in the axial direction. Similarly, taking the axial component of the second term of the right-hand side yields,

$$e_z\cdot\mu\{\nabla\langle v\rangle+\nabla\langle v\rangle^T\}\cdot\nabla(1-\varepsilon)=-2\mu\left(\frac{\partial\langle v\rangle_z}{\partial z}\frac{\partial\varepsilon}{\partial z}\right). \tag{26}$$

Except near the sparger, the quantities $\langle v\rangle_z$ and ε change only modestly with axial position. The second derivative of $\langle v\rangle_z$ is expected to be at least as small as its first derivative. However, the change in $\langle v\rangle_z$ with r is considerable. Consequently, axial derivative may be considered to be negligible relative to the radial derivative, and the axial component of the viscous term may be expressed approximately as,

$$(1-\varepsilon)\mu\left[\frac{1}{r}\frac{\partial}{\partial r}\left(r\frac{\partial\langle v\rangle_z}{\partial r}\right)\right]. \tag{27}$$

For the turbulent stress term, the dot product with e_z has the form of the z component of the divergence of a dyad

$$\begin{aligned}&e_z\cdot(\nabla(1-\varepsilon)\langle\overline{\rho v'v'}\rangle)\\&\quad=\left\lfloor\nabla\cdot(1-\varepsilon)\langle\overline{\rho v'v'}\rangle\right\rfloor_z\\&\quad=\frac{1}{r}\frac{\partial}{\partial r}(r(1-\varepsilon)\cdot\langle\overline{\rho v_r'v'}_z\rangle)+\frac{1}{r}\frac{\partial(1-\varepsilon)\langle\overline{\rho v_\theta'v_z'}\rangle}{\partial\theta}\\&\qquad+\frac{\partial((1-\varepsilon)\langle\overline{\rho v_z'v_z'}\rangle)}{\partial z}.\end{aligned} \tag{28}$$

If the flow is assumed to be symmetrical with respect to azimuthal position, the second term on the right-hand side is zero. Further, changes in v_z with axial position are expected to be small, and the z derivative term is assumed to be negligible. Consequently, the axial component of the Reynolds stress term becomes,

$$\frac{1}{r}\frac{\partial}{\partial r}(r(1-\varepsilon)\langle\overline{\rho v_r'v_z'}\rangle). \tag{29}$$

The momentum equation in the axial direction can be averaged over the cross-sectional area of the riser to eliminate radial dependencies,

$$\begin{aligned}&-\frac{1}{A}\int_A\left[\frac{\partial}{\partial z}((1-\varepsilon)\langle P\rangle)\right]dA-\frac{1}{A}\int_A((1-\varepsilon)\langle\rho\rangle g_z)\,dA\\&\quad+\frac{1}{A}\int_A\left[(1-\varepsilon)\mu\left(\frac{1}{r}\frac{\partial}{\partial r}\left(r\frac{\partial\langle v\rangle_z}{\partial r}\right)\right)\right]dA\\&\quad+\frac{1}{A}\int_A\left[\frac{1}{r}\frac{\partial}{\partial r}(r(1-\varepsilon)\langle\overline{\rho v_r'v_z'}\rangle)\right]dA+\frac{1}{A}\int_A a_{lg}F_t\,dA=0.\end{aligned} \tag{30}$$

The pressure is virtually independent of radial position and can be removed from the area integral. Reversing the order of integration and differentiation for the pressure term then gives,

$$-\frac{1}{A}\int_A\frac{\partial}{\partial z}[(1-\varepsilon)\langle P\rangle]\,dA=-\frac{\partial}{\partial z}[\langle P\rangle(1-\hat{\varepsilon})]. \tag{31}$$

The gravity term may be evaluated similarly since the density is also independent of radial position. In evaluating the viscous term, the time-averaged gas volume fraction ε is written as the sum of the cross-sectional average and its deviation. Substitution into the viscous term results in the expression,

$$\frac{\mu}{\pi R^2}\int_0^{2\pi}\int_0^R (1-\varepsilon)\left(\frac{1}{r}\frac{\partial}{\partial r}\left(r\frac{\partial\langle v\rangle_z}{\partial r}\right)\right) r\,\mathrm{d}r\,\mathrm{d}\theta = \frac{2\pi}{R^2}(1-\hat{\varepsilon})R\left(\frac{\partial\langle v\rangle_z}{\partial r}\right)\Big|_R - \frac{2\mu}{R^2}\int_0^R \varepsilon\,\mathrm{d}\left(r\frac{\partial\langle v\rangle_z}{\partial r}\right). \quad (32)$$

The first term on the right-hand side represents the viscous part at the wall based on gradients in the averaged velocity. The second term is assumed to be negligible based on the relative magnitudes of $(1-\hat{\varepsilon})$ and $\breve{\varepsilon}$. The turbulent stress term may be integrated to obtain,

$$\frac{1}{2R^2}\int_0^{2\pi}\int_0^R \left[\frac{1}{r}\frac{\partial}{\partial r}(r(1-\varepsilon)\langle\overline{\rho v_r' v_z'}\rangle)\right] r\,\mathrm{d}r\,\mathrm{d}\theta = \frac{2}{R}(1-\varepsilon)\langle\overline{\rho v_r' v_z'}\rangle|_R, \quad (33)$$

which represents the turbulent stresses at the wall. The combined viscous and turbulent wall drag may be represented in a traditional friction factor form as,

$$\frac{f_r}{D}\frac{1}{2}\rho\langle\hat{v}\rangle_z^2. \quad (34)$$

Lastly, the interfacial drag term F_{bz} is expressed as the sum of its cross-sectional average and a deviation. Noting that the integral of the deviation over the cross-section is zero, the gas–liquid drag term can be shown to have the form,

$$\frac{3}{Ar_b}\int_A F_{bz}\varepsilon\,\mathrm{d}A = a_{lg}F_t + \frac{3}{Ar_b}\int_A \breve{F}_{bz}\breve{\varepsilon}\,\mathrm{d}A. \quad (35)$$

Assuming that the integral of the product of the deviations is small compared to the product of the averages, the final form of the one-dimensional momentum equation for the liquid is,

$$-\frac{\mathrm{d}}{\mathrm{d}z}[\langle P\rangle(1-\hat{\varepsilon})] - (1-\hat{\varepsilon})\langle\rho\rangle g_z - \frac{f_r}{D}\frac{1}{2}\rho\langle\hat{v}\rangle_z^2 + a_{lg}F_t = 0. \quad (36)$$

The total vertical force per unit area at the gas–liquid interface can be expressed as the difference between downward drag and viscous forces per unit area (F_d), and upward forces due to hydrostatic pressure variations per unit area (F_b),

$$F_t = F_d - F_b. \quad (37)$$

To quantify F_b we will explore hydrostatic pressure effects at the gas–liquid interface in a control volume of length dz in the riser, as depicted in Fig. 2. From this representation, it can be seen that F_d corresponds to the total buoyancy forces exerted on the bubbles contained in the control volume per unit gas–liquid interfacial area minus the external pressure forces exerted on the gas at the top and bottom sections of the control volume per unit gas–liquid interfacial area,

$$F_b = \frac{\bar{\varepsilon}\rho_l g}{\bar{a}_{lg}} + \frac{(\langle\bar{P}_g\rangle A_g)|_{z+dz} - (\langle\bar{P}_g\rangle A_g)|_z}{V\bar{a}_{lg}}, \quad (38)$$

where in this case V is the control volume ($V = A\,\Delta z$). If we consider that $\bar{\varepsilon} = A_g/A$, and take the limit as $\Delta z \to 0$, we obtain,

$$\bar{F}_b = \frac{\bar{\varepsilon}\rho_l g}{\bar{a}_{lg}} + \frac{1}{\bar{a}_{lg}}\frac{\mathrm{d}(\langle\bar{P}_g\rangle\bar{\varepsilon})}{\mathrm{d}z}. \quad (39)$$

Pressure differences between gas and liquid phases can only be due to the pressure jump across the bubble surfaces due to surface tension effects. It can be shown that the pressure jump is appreciably lower than the values of gas and liquid pressures. Therefore, we will assume that liquid and gas pressures within an averaging volume are approximately the same. To a good degree of approximation we can then state,

$$\langle\bar{P}_g\rangle = \langle\bar{P}_l\rangle = \langle\bar{P}\rangle. \quad (40)$$

By using this fact, we then obtain from the above equations, the liquid-phase momentum equation,

$$-\frac{\mathrm{d}\langle\bar{P}\rangle}{\mathrm{d}z} - \rho_l g - \frac{f_r}{D}\frac{1}{2}\rho_l\langle\bar{v}_l\rangle^2 + \bar{a}_{lg}\bar{F}_d = 0. \quad (41)$$

The friction factor was determined from empirical correlation used by Young et al. [15],

$$f_r = \frac{0.187\sqrt{\bar{\varepsilon}}}{(1-\bar{\varepsilon})^{0.10}}\left(\frac{\sqrt{gD}}{\langle V_z\rangle}\right)^{1.1}. \quad (42)$$

A similar approach can be followed for the gas-phase momentum equation. After applying the volume averaging technique to the time-averaged point equation of motion for $i = g$, it is possible to show that the averaged gas-phase momentum equation can be written as follows:

$$\frac{\mathrm{d}(\bar{\varepsilon}\langle\bar{P}\rangle)}{\mathrm{d}z} - \bar{a}_{lg}\bar{F}_t = 0, \quad (43)$$

where gravitational effects have been neglected due to the relatively low density of the gas phase. So finally from the above equations we get,

$$\bar{\varepsilon}\rho_l g = \bar{a}_{lg}\bar{F}_d. \quad (44)$$

This final form of the gas phase momentum equation states that buoyancy balances the total drag and viscous forces at the gas–liquid interface. Therefore, the contribution of interfacial drag and viscous forces to the liquid momentum equation can be replaced by the buoyancy force, which yields,

$$-\frac{\mathrm{d}\langle\bar{P}\rangle}{\mathrm{d}z} - (1-\bar{\varepsilon})\rho_l g - \frac{f_r}{D}\frac{1}{2}\rho_l\langle\bar{v}_l\rangle^2 = 0. \quad (45)$$

This equation states that the pressure gradient in the liquid phase is due to hydrostatic contributions of the liquid holdup plus pressure losses due to wall friction.

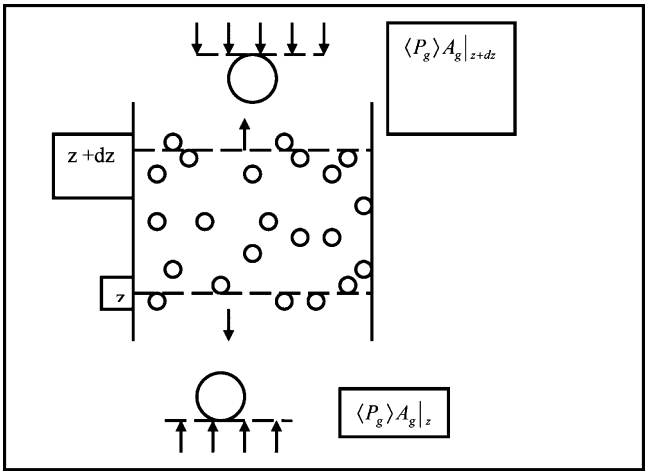

Fig. 2. Control volume used to determine hydrostatic forces at the gas–liquid interface (dotted lines) in a section of riser.

2.3. Separator

The mechanical energy balance was employed to analyze the separator liquid-phase flow. Analysis begins with the time-averaged differential mechanical energy equation for steady flow in a fixed control volume,

$$\int_{A_e}\frac{1}{2}\rho v^2(v\cdot n)\,\mathrm{d}A = \int_{A_e} v\cdot(n\cdot T^{(T)})\,\mathrm{d}A - \int_{A_e}\rho\phi(v\cdot n)\,\mathrm{d}A - \dot{E}_v, \quad (46)$$

where $v = \sqrt{v_r^2 + v_\theta^2 + v_z^2}$, $T^T = -Pn + ([\tau + \tau^t] \cdot n)$, A_e is the cross-sectional flow areas at entrances and exits, n is the unit vector outwardly normal to A_e, φ is the gravitational potential, and E_v is the rate of viscous dissipation.

Since the bulk flow at both the riser and the downcomer entrance is in the axial direction, the time-averaged radial and azimuthal velocity components are small compared to v_z. Hence, $v_{z\,dc} \approx \sqrt{v_z^2} = v_z$. In the downcomer, measurements showed that the radial dependence of v_z is weak, and $v_z = v_{z\,dc}$ to a good approximation. The radial dependence is greater in the riser. By expressing the riser volume-averaged velocity as an area average and a deviation, and assuming that the higher order terms of the velocity deviation are negligible compared to $\langle v \rangle_z$, the first term in the mechanical energy balance can be shown to have the form:

$$\int_{A_e} \frac{1}{2}\rho v^2 (v \cdot n)\, dA = \frac{\rho}{2}\hat{v}_{z\,dc}^3 A_{dc} - \frac{\rho}{2}\langle \hat{v} \rangle_z^3 A_r (1 - \hat{\varepsilon}). \tag{47}$$

The second integral in the mechanical energy balance may be expanded by substituting the expression for the total stress vector:

$$\int_{A_e} v \cdot (n \cdot T^T)\, dA = \int_{A_e} v \cdot (-Pn)\, dA + \int_{A_e} (v \cdot \tau \cdot n)\, dA + \int_{A_e} (v \cdot \tau^t \cdot n)\, dA. \tag{48}$$

To a very good approximation, the time-averaged pressure is independent of radial position. The pressure integral term becomes:

$$-\int_{A_e} P(v \cdot n)\, dA \approx (\hat{v}_z A)_{dc} + [\langle P \rangle \langle \hat{v} \rangle_z (1 - \hat{\varepsilon}) A]_r. \tag{49}$$

Using index notation, the viscous stress term for the downcomer may be shown to have the form

$$v \cdot \tau \cdot n = v_z \left[2\mu \left(\frac{\partial v_z}{\partial z} \right) \right] \tag{50}$$

assuming again that the axial acceleration of the flow is negligible in comparison to the pressure and inertial terms. An analogous treatment holds for the riser term. The turbulent stress term reduces to the form:

$$(v \cdot \tau^t \cdot n) = v_z \rho l_{zz}^2 \left| \frac{\partial v_z}{\partial z} \right| \left(\frac{\partial v_z}{\partial z} \right), \tag{51}$$

where l_{zz} is the Prandtl mixing length of unknown magnitude. The upper limit of the mixing length may be estimated to be a bubble diameter. Since velocity changes in the z direction are small, the turbulent stress term may also be assumed to be small relative to the P and $\hat{v}_z^3$ terms. Again, an analogous development holds for the riser.

Evaluation of the gravity term over entrance and exit yields,

$$\int_{A_e} \rho\phi (v \cdot n)\, dA = -\rho\phi \langle \hat{v} \rangle_{zr} A_r (1 - \hat{\varepsilon}) + \rho\phi \hat{v}_{z\,dc} A_{dc}. \tag{52}$$

Substitution of the above terms into the original form of the mechanical energy balance results in the expression:

$$\frac{\rho}{2}\hat{v}_{z\,dc}^3 A_{dc} - \frac{\rho}{2}\langle \hat{v} \rangle_z^3 A_r (1 - \hat{\varepsilon}) = -(P\hat{v}_z A)_{dc} + (\langle P \rangle \langle \hat{v} \rangle_z (1 - \hat{\varepsilon}) A)_r + \rho\phi \langle \hat{v} \rangle_{zr} A_r (1 - \hat{\varepsilon}) - \rho\phi \hat{v}_{z\,dc} A_{dc} - \dot{E}_v. \tag{53}$$

By substitution of the continuity relationship:

$$\rho \hat{v}_{z\,dc} A_{dc} = \rho \langle \hat{v} \rangle_{zr} (1 - \widehat{\varepsilon}) A_r \tag{54}$$

and division by $\rho g v_{z\,dc} A_{dc}$ the separator mechanical energy equation becomes,

$$\frac{\hat{v}_{z\,dc}^2}{2g}\left[1 - \frac{1}{(1 - \hat{\varepsilon})^2}\left(\frac{D_{dc}}{D_r} \right)^2 \right] - \frac{\langle \hat{P} \rangle_r - \hat{P}_{dc}}{\rho g} + \frac{\dot{E}_v}{\rho g \hat{v}_{z\,dc} A_{dc}} = 0. \tag{55}$$

The last term is frequently referred to as the minor head loss term h_m and is represented as the product of a loss factor K times the ratio of the characteristic kinetic energy per unit volume to the gravity force per unit volume, i.e., $h_m = Kv^2/2g$. One can estimate the loss factors for expansion into the separation tank and contraction into the downcomer as,

$$K = \left[1 - \left(\frac{D_r}{D_t} \right)^2 \right]^2 \quad \text{and} \quad K = 0.5, \tag{56}$$

respectively. The quantity D_t is the equivalent diameter of the separation tank, which was set equal to the width of the rectangular tank base. Incorporating the minor loss terms and simplifying the use of the continuity equation, the macroscopic momentum balance for the separation chamber has the final form:

$$\frac{\hat{v}_{z\,dc}^2}{2g}\left[\frac{3}{2} + \left(\frac{D_{dc}}{(1 - \hat{\varepsilon}) D_r} \right)^2 \left(\left[1 - \left(\frac{D_r}{D_t} \right)^2 \right]^2 \left(\frac{D_{dc}}{D_r} \right)^2 - 1 \right) \right] + \frac{\langle \hat{P} \rangle_r - \hat{P}_{dc}}{\rho g} = 0. \tag{57}$$

The liquid-phase continuity equation may be applied to the separation chamber with the following intuitive result equating the influx from the riser and the efflux to the downcomer:

$$\rho (1 - \varepsilon)_r \langle v \rangle_{zr} A_r = \rho \hat{v}_{z\,dc} A_{dc}. \tag{58}$$

2.4. Downcomer

For modeling purposes the downcomer section is defined as the flow channel extending from the separator exit to the sparger. As previously noted, the downcomer flow is assumed to be all liquid. The mechanical energy balance was applied to the downcomer in a manner analogous to the separation chamber derivation. Following the same arguments made for the separator and noting the changed orientation of the velocity and unit normal vectors, the three integrals of the differential energy balance can be shown to simplify to the following forms:

$$\int_{A_e} \frac{1}{2}\rho v^2 (v \cdot n)\, dA = -\frac{\rho}{2}\widehat{v}_{z_{dc}}^3 A_{dc} + \frac{\rho}{2}\langle \widehat{v} \rangle_{Z_r}^3 (1 - \widehat{\varepsilon}) A_r, \tag{59}$$

$$\int v \cdot (n \cdot T^{(T)})\, dA = P_{dc} \hat{v}_{z\,sc} A_{dc-} \langle P \rangle_r \langle \hat{v} \rangle_{zr} (1 - \hat{\varepsilon}) A_r, \tag{60}$$

$$\int_{A_e} \rho\phi (v \cdot n)\, dA = -\rho\phi_{dc} \hat{v}_{zdc} A_{dc} + \rho\phi_r \langle \hat{v} \rangle_{zr} (1 - \hat{\varepsilon}) A_r. \tag{61}$$

Collecting terms, the mechanical energy balance becomes:

$$\frac{\rho}{2}\langle \hat{v} \rangle_{zr}^3 (1 - \hat{\varepsilon}) A_r - \frac{\rho}{2}\hat{v}_{zdc}^3 A_{dc} = P_{dc} \hat{v}_{z\,dc} A_{dc} - \langle P \rangle_r \langle \hat{v} \rangle_{zr} (1 - \hat{\varepsilon}) A_r + \rho\varphi_{dc} \hat{v}_{z\,dc} A_{dc} - \rho\varphi_r \langle \hat{v} \rangle_{zr} (1 - \hat{\varepsilon}) A_r - \dot{E}_v. \tag{62}$$

The gravity potential terms may be simplified using the relationship,

$$\phi_{dc} - \phi_r = \int_0^L g\,dz = gL. \tag{63}$$

By incorporating the continuity relationship between the downcomer and riser velocities and dividing by $\rho g \hat{v}_{z\,dc} A_{dc}$, the downcomer mechanical energy equation takes the form,

$$\frac{\hat{v}_{z\,dc}^2}{2g}\left[\left(\frac{D_{dc}}{D_r}\right)^2 - 1\right] = \frac{P_{dc} - \langle P\rangle_r}{\rho g} + L - \frac{\dot{E}_v}{\rho g \hat{v}_{z\,dc} A_{dc}}. \tag{64}$$

The last term may be represented as the sum of the frictional loss h_f and the minor losses h_m. The frictional losses are commonly written in the form of Darcy–Weisbach formula,

$$h_f = f_{dc}\left(\frac{L}{D}\right)_{dc}\frac{\hat{v}_{z\,dc}^2}{2g}. \tag{65}$$

The minor losses may be depicted using K loss factors as before. Young et al. [15] lists the following values,

$$\begin{aligned} &K\ (90^\circ\ \text{elbow with meter}) = 1.3,\\ &K\ (\text{expansion from downcomer to riser}) = \left[1 - \left(\frac{D_{dc}}{D_r}\right)^2\right]^2,\\ &K\ (\text{tee used as ell entering through branch}) = 1.5. \end{aligned} \tag{66}$$

Incorporating these empirical expressions, the macroscopic mechanical energy balance for the downcomer has the final form,

$$\frac{\hat{v}_{z\,dc}^2}{2g}\left[\left[\left(\frac{D_{dc}}{D_r}\right)^2 - 1\right] + \frac{\langle P\rangle_r - P_{dc}}{\rho g} - L + f_{dc}\left(\frac{L}{D}\right)_{dc}\frac{\hat{v}_{z\,dc}^2}{2g}\right.$$
$$\left.\left\{1.3 + \left[1 - \left(\frac{D_{dc}}{D_r}\right)^2\right]^2\right\} + 1.5\frac{\langle \hat{v}_{zr}^2\rangle}{2g} = 0\right]. \tag{67}$$

Simplifying this we obtain the final equation as,

$$\left\{\left[\left(\frac{D_{dc}}{D}\right)^2 - 1\right] + f_{dc}\frac{L_{dc}}{D_{dc}} + \sum_i K_i\right\}\frac{\bar{v}_{dc}^2}{2g} + \frac{\langle \bar{P}\rangle_{z=0} - \bar{P}_{dc,z=L}}{\rho_l g} - L = 0. \tag{68}$$

3. Implementation of the model

For solving the model, the basic information that must be available consists of: the riser and downcomer lengths L and L_{dc}, the riser and downcomer diameters D and D_{dc}, physical properties of the fluids (ρ_l, ρ_g, μ_l, σ), atmospheric pressure P_a, operating temperature T, the liquid level in the gas–liquid separator h_t, the bubble radius at the sparger r_{b0} ($z = 0$), and the gas superficial mass velocity (gas mass flow rate per unit cross-sectional area L_g).

Integrating the liquid-phase continuity equation yields,

$$\rho_l(1 - \bar{\varepsilon})\langle \bar{v}_l\rangle = L_f, \tag{69}$$

where L_f is the superficial mass velocity of the liquid phase (liquid mass flow rate per unit cross-sectional area), whose value is independent of axial position. This value represents the mass of liquid per unit time and unit riser area that is circulating through the system, which is not known a priori. The solution procedure starts by assuming a value for L_f.

Integrating the gas-phase continuity equation after using the ideal gas equation yields:

$$\frac{\langle \bar{P}\rangle M_g}{RT}\bar{\varepsilon}\langle \bar{v}_g\rangle = L_g, \tag{70}$$

where L_g is the superficial mass velocity of the gas phase, which is also independent of axial position.

The pressure at the top of the riser is calculated from the following equation:

$$\langle \bar{P}\rangle_{z=L} = P_a + \rho_l g h_t. \tag{71}$$

Once L_f is known, the gas-phase momentum equation combined with the appropriate drag coefficient correlation, along with the above two integrated equations evaluated at the top of the riser ($z = L$) represent a system of three non-linear algebraic equations with three unknowns: the gas and liquid velocities, and the gas holdup. These equations are solved and the results constitute a starting point for the integration of the liquid-phase momentum equation.

The differential equation was solved in MATLAB using the standard function "ode45". The first sets of non-linear algebraic equations were solved using the function "fsolve". Solving the ODE we get the local values of liquid and gas velocities and gas holdup.

Once the pressure, velocities, and gas holdup at the sparger are known, the mechanical energy balance in the downcomer is used to calculate v_{dc}. A new value of L_f is then found by combining the integrated liquid phase continuity equation with the macroscopic mass balance equation in the separator. If this value is different from the one used in the previous iteration, a new value for L_f is assigned and the iteration procedure continues. When the procedure converges, the solution gives the pressure, phase velocities, gas holdup and bubble radius profiles in the riser (bubble radii are not calculated in this investigation).

In this model we have used the following drag coefficient correlation:

$$\hat{C}_d = \frac{4}{3} r_b \sqrt{\frac{g(\rho_l - \rho_g)}{\sigma(1 - \varepsilon)}}. \tag{72}$$

The important thing about this approach is that this model does not require the specification of a boundary condition for the gas holdup, since the only differential equation has the average pressure as a dependent variable, for which the equation $\langle \bar{P}\rangle_{z=L} = P_a + \rho_l g h_t$ acts as the only necessary boundary condition.

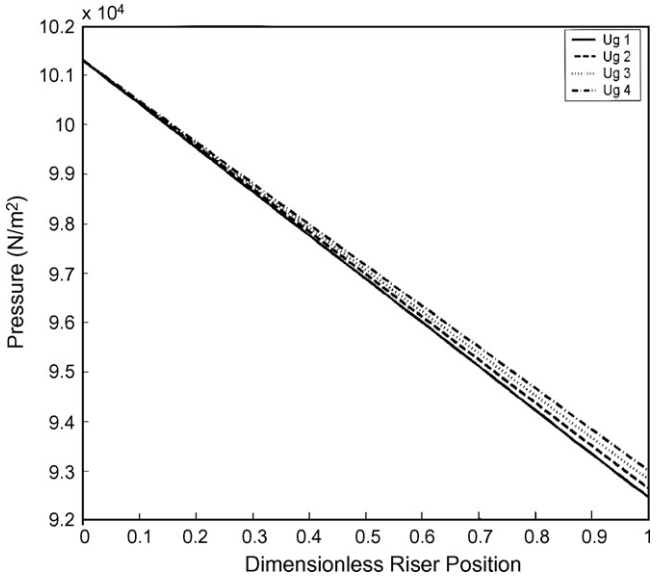

Fig. 3. Pressure profiles, for different superficial gas velocity, as a function of dimensionless riser position.

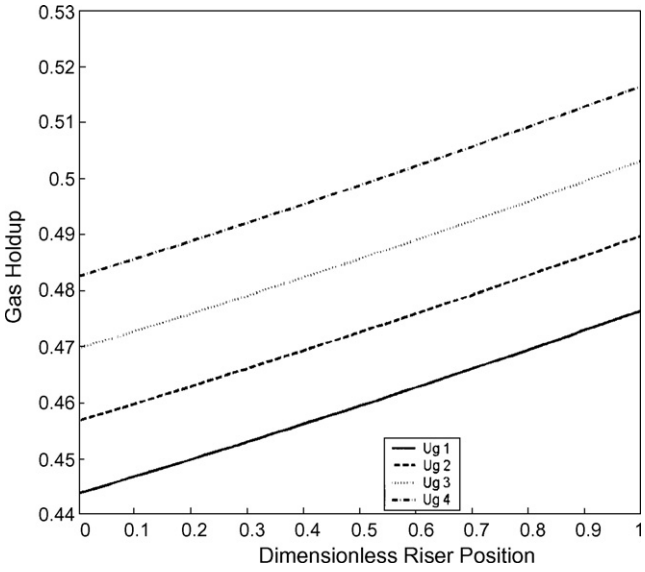

Fig. 4. Effect of dimensionless riser position on gas holdup for different superficial gas velocities.

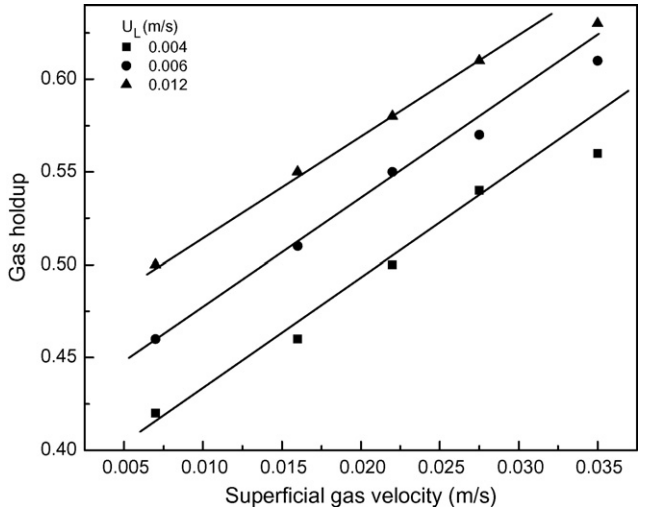

Fig. 5. Comparison of predicted gas holdup with that of experimental results.

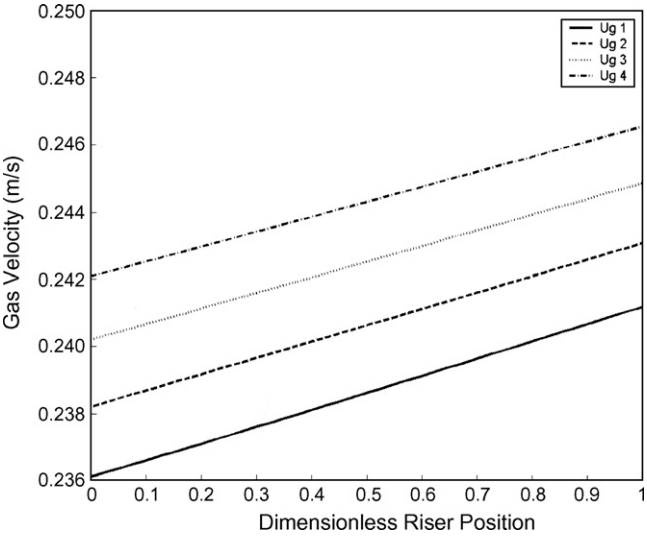

Fig. 6. Effect of dimensionless riser position on gas velocity for different U_g values.

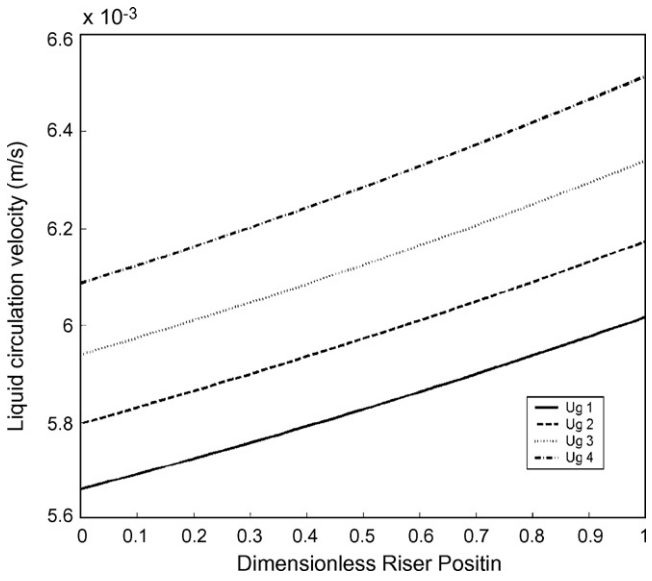

Fig. 7. Effect of dimensionless riser position on liquid circulation velocity for different superficial gas velocities.

4. Results and discussion

The results obtained after solving the model equations using MATLAB are presented in Figs. 3–7. The variations of pressure, gas holdup, liquid velocity and gas velocity are obtained as a function of the dimensionless riser position.

Fig. 3 shows the predicted pressure profiles as a function of the dimensionless riser positions for four different superficial gas velocities. The pressures were calculated for four different values of the superficial gas velocity. It can be noted that, the change in pressure drop is not significant with the riser position. The predicted pressure drop is well in the range reported by Mohanty et al. [5].

Fig. 4 shows the variations of predicted gas holdup with the riser position. From Fig. 4 we see that the variation of the gas holdup with riser position is almost insignificant. That is, if we go up the riser starting from the bottom, there would not be much difference in the gas holdup. However, the gas holdup increases with the increase in superficial gas velocity for a particular riser position. The values of gas holdup obtained are in the range of 0.44–0.52. Fig. 5 shows a comparison of the predicted gas holdup profile along with that of experimental data reported in literature [5]. The lines represent the predicted gas holdup values from the model and the points represent the experimental data. It can be seen that, the predicted values are in excellent agreement with the experimental results reported by Mohanty et al. [5] for the same range of operating parameters.

Fig. 6 shows the predicted gas velocity profiles as a function of the dimensionless riser position for four different superficial gas velocities. The results obtained for the gas velocities can be interpreted in a similar fashion as mentioned above.

The effect of dimensionless riser position on liquid circulation velocity for four different gas velocities are presented in Fig. 7. In this case also, the riser position does not have a significant effect on liquid circulation velocity. However, with increase in gas velocity for a constant riser position, the liquid circulation velocity increases. The increase in gas velocity results in a large driving force that forces the liquid to the downcomer, thereby increasing the liquid circulation velocity.

5. Conclusions

A model to describe the multi-stage external loop airlift reactor hydrodynamics has been developed in this work. The unique feature of this reactor is the multi-stage system. Starting from time-averaged point equation of continuity, and using the mass and momentum balance equations the model formulation has been carried out by applying an averaging technique over a representative volume of gas–liquid suspension. The main advantage of this model is that its simulation of the riser requires the solution of only one differential equation, the liquid-phase momentum equation. This eliminates the need for a boundary condition for the gas holdup, which is very difficult to formulate on physical grounds. Results indicate that the predicted hydrodynamic values from model agreed well with that of experimental values reported in the literature. If the drag coefficient is taken as an explicit function of the Reynolds number, knowledge of the bubble size at the sparger is required to determine the pressure, gas holdup and phase velocity profiles in the riser. The model is sensitive to the initial value of the bubble size.

References

[1] M.Y. Chisti, M. Moo-Young, Airlift reactors: characteristics, applications and design considerations, Chem. Eng. Commun. 60 (1987) 195–242.
[2] M.Y. Chisti, Airlift Bioreactors, Elsevier, London, 1989.
[3] H. Dhaouadi, S. Poncin, J.M. Hornut, G. Wild, P. Oinas, Hydrodynamics of an airlift reactor: experiments and modeling, Chem. Eng. Sci. 51 (1996) 2625–2630.
[4] J. Merchuk, M.H. Siegel, Airlift reactors in chemical and biological technology, J. Chem. Technol. Biotechnol. 41 (1988) 105–120.
[5] K. Mohanty, D. Das, M.N. Biswas, Hydrodynamics of a novel multi-stage external loop reactor, Chem. Eng. Sci. 61 (2006) 4617–4624.
[6] M.Y. Chisti, B. Halard, M. Moo-Young, Liquid circulation in airlift reactors, Chem. Eng. Sci. 43 (1988) 451–457.
[7] E. Garcia-Calvo, P. Leton, Prediction of gas hold-up and liquid velocity in airlift reactors using two-phase flow friction coefficients, J. Chem. Technol. Biotechnol. 67 (1996) 388–396.
[8] Z. Kemblowski, J. Przywarski, A. Diab, An average gas hold-up and liquid circulation velocity in airlift reactors with external loop, Chem. Eng. Sci. 48 (1993) 4023–4035.
[9] C. Freitas, M. Fialova, J. Zahradnik, J.A. Teixeira, Hydrodynamic model for three-phase internal- and external-loop airlift reactors, Chem. Eng. Sci. 54 (1999) 5253–5258.
[10] N. Zuber, J.A. Findlay, Average volume concentration in two phase flow systems, J. Heat Transf. Ser. C 87 (1965) 453–468.
[11] J. Merchuk, Y. Stein, Local hold-up and actual liquid velocity in air-lift reactors, AIChE J. 27 (1981) 377–388.
[12] P. Verlaan, J. Tramper, K. vant Riet, K.C.A.M. Luyben, Hydrodynamics and axial dispersion in an airlift-loop bioreactor with two and three phase flow, in: Proceedings of the International Conference on Bioreactor Fluid Dynamics, Cambridge, England, April 15–17, 1986, pp. 93–107.
[13] B.C. Meikap, G. Kundu, M.N. Biswas, Scrubbing of fly-ash laden SO_2 in a modified multi-stage bubble column scrubber, AIChE J. 48 (2002) 2074–2083.
[14] S. Becker, A. Sokolichin, G. Eigenberger, Gas–liquid flow in bubble column and loop reactors. Part II. Comparison of detailed experiments and flow simulations, Chem. Eng. Sci. 49 (1994) 5747–5762.
[15] M.A. Young, R.G. Carbonell, D.F. Ollis, Airlift bioreactor: analysis of local two-phase hydrodynamics, AIChE J. 37 (1991) 403–428.
[16] G. Hillmer, L. Weismantel, H. Hofmann, Investigations and modeling of slurry bubble columns, Chem. Eng. Sci. 49 (1994) 837–843.
[17] S. Sarkar, B.C. Meikap, S.G. Chatterjee, Modeling of removal of sulfur dioxide from flue gases in a horizontal cocurrent gas–liquid scrubber, Chem. Eng. J. 131 (2007) 263–271.